Evaluation of morphological and hemodynamic biomarkers to assess rupture risk of intracranial aneurysms using magnetic resonance fluid dynamics and computational fluid dynamics

(脳動脈瘤破裂リスク評価のための磁気共鳴流体解析と計算流体解析による形態ならびに血流動態バイオマーカーの検討)

Nagoya University Graduate School of Medicine

Department of Radiological and Medical Laboratory Sciences

名古屋大学大学院医学系研究科

医療技術学専攻

Majuwana Gamage Roshani Sandamini Perera

2019 年度学位申請論文

Evaluation of morphological and hemodynamic biomarkers to assess rupture risk of intracranial aneurysms using magnetic resonance fluid dynamics and computational fluid dynamics
(脳動脈瘤破裂リスク評価のための磁気共鳴流体解析と計算流体解析による形態ならびに血流動態バイオマーカーの検討)

名古屋大学大学院医学系研究科

医療技術学専攻

（指導教員 ： 礒田 治夫 教授）

Majuwana Gamage Roshani Sandamini Perera

Abstract

Purpose

Evaluate in-vivo hemodynamic and morphological biomarkers of intracranial aneurysms, using magnetic resonance fluid dynamics (MRFD) and MR based patient specific computational fluid dynamics (CFD) in order to assess the risk of rupture.

Methods

Forty-eight intracranial aneurysms (10 ruptured, 38 unruptured) were scrutinized for 6 morphological and 10 hemodynamic biomarkers. Morphological biomarkers were calculated based on 3D time-of-flight magnetic resonance angiography (3D TOF MRA) in MRFD analysis. Hemodynamic biomarkers were assessed using both MRFD and CFD analyses. MRFD was performed using 3D TOF MRA and 3D cine phase-contrast magnetic resonance imaging (3D cine PC MRI). CFD was performed utilizing patient specific inflow-outflow boundary conditions derived from 3D cine PC MRI. Univariate analysis was carried out to identify statistically significant biomarkers for aneurysm rupture and receiver operating characteristic (ROC) analysis was performed for the significant biomarkers. Binary logistic regression was performed to identify independent predictive biomarkers.

Results

Morphological biomarker analysis revealed that aneurysm size [p = 0.021], volume [p = 0.035] and size ratio [p = 0.039] were statistically significantly different between the two groups. In hemodynamic biomarker analysis, MRFD results indicated that ruptured aneurysms had higher oscillatory shear index (OSI) [OSI.max, p = 0.037] and higher relative residence time (RRT) [RRT.ave, p = 0.035] compared to unruptured aneurysms. Correspondingly CFD analysis demonstrated significant differences for both average and maximum OSI [OSI.ave, p = 0.008; OSI.max, p = 0.01] and maximum RRT [RRT.max, p = 0.045]. ROC analysis revealed AUC values greater than 0.7 for all significant biomarkers. Aneurysm volume [AUC,0.718; 95%CI, 0.491-0.946] and average OSI obtained from CFD [AUC, 0.774; 95%CI, 0.586-0.961] were retained in the respective logistic regression models.

Conclusions

Both morphological and hemodynamic biomarkers have significant influence on intracranial aneurysm rupture. Aneurysm size, volume, size ratio, OSI and RRT could be potential biomarkers to assess aneurysm rupture risk.

要旨

目的

脳動脈瘤の破裂リスクを評価するため、「磁気共鳴流体解析（MRFD)」と「磁気共鳴（MR）に基づく患者固有の計算流体解析（CFD)」を施行し、脳動脈瘤の生体内血流動態バイオマーカーと形態バイオマーカーを評価した。

方法

48 個の脳動脈瘤（破裂 10 個、未破裂 38 個）を解析対象とし、形態バイオマーカー6 個と血流動態バイオマーカー10 個を各動脈瘤群で比較した。 形態バイオマーカーは 3 次元タイムオブフライト磁気共鳴血管像（3D TOF MRA）データから MRFD を施行して求めた。血流動態バイオマーカーは MRFD と CFD の両者を施行して評価した。MRFD は 3D TOF MRA と 3D シネ位相コントラスト磁気共鳴画像（3D cine PC MR）を使用して解析した。CFD は 3D cine PC MR データから得られた患者固有の流入流出境界条件を用いて解析した。 統計的に有意差のある動脈瘤破裂のバイオマーカーを特定するため単変量解析を実施し、統計的に有意差のあるバイオマーカーに対して ROC 解析を実施した。 独立した予測バイオマーカーを同定するため、2 値ロジスティック回帰を施行した。

結果

形態バイオマーカーの解析では、破裂脳動脈瘤は未破裂脳動脈瘤と比べて、動脈瘤最大径［p=0.021]、動脈瘤体積［p=0.035]、サイズ比（動脈瘤頸部径/親動脈径の比）[p=0.039］が各々統計的に有意に大きかった。MRFD から求めた血流動態バイオマーカーの結果から、破裂動脈瘤は未破裂脳動脈瘤と比べて、振動せん断指数（OSI）[OSI.max、p = 0.037］と相対滞留時間（RRT）[RRT.ave、p = 0.035］が高かった。同様に、CFD の結果から、平均 OSI と最大 OSI の両者［OSI.ave、p = 0.008; OSI.max、p = 0.01］と最大 RRT ［RRT.max、p = 0.045］で有意差が示された。 ROC 解析では統計的に有意差のあった全てのバイオマーカーの曲線下面積（AUC）値は 0.7 を超えた。また、動脈瘤体積［AUC、0.718; 95%CI、0.491-0.946］と CFD から得られた平均 OSI［AUC、0.774; 95%CI、0.586-0.961］はそれぞれ独立した脳動脈瘤破裂の予測バイオマーカーであった。

結論

形態と血流動態の両者のバイオマーカーは、脳動脈瘤破裂に大きな影響を及ぼす。脳動脈瘤最大径、動脈瘤体積、サイズ比、OSI と RRT は脳動脈瘤破裂を予測できる有望なバイオマーカーと考えられる。

Table of Contents

Introduction

Intracranial aneurysms

Intracranial aneurysms (IAs) are pathological dilatations of the arterial walls and an estimated overall prevalence of 3.2% has been reported for a non-comorbid population [1]. Commonly encountered types of IAs are saccular aneurysms and fusiform aneurysms. Saccular aneurysms, which is the most common kind of IAs, are pouch-like or berry shaped pathological dilatations [2-3]. Fusiform aneurysms are non-saccular dilatations which comprise the entire vessel wall for a short distance [4].

IAs and Hemodynamics

Hemodynamics refers to the physical study of flowing blood and its vessels in the research context while this term is simply used in clinical practice to refer basic measures of cardiovascular functions [5]. Hemodynamic forces, with respect to the former referral, are considered as regulating factors of blood vessel structure and influence formation of vascular pathology such as atherosclerosis, aneurysms and arteriovenous malformations [6]. Many researchers have proposed that hemodynamics, such as wall shear stress (WSS) [6] and its derivatives [7-12], can be a causative factor in aneurysm pathophysiology, which plays a fundamental role in the mechanisms of growth and rupture as well. IAs are thought to be formed when the arterial walls are unable to resist the hemodynamic forces, as a result of tunica media thinning, and distend [2,13]. Progress of aneurysms is also thought to be driven by hemodynamics, where it provides mechanical triggers which are transduced into biological signals leading to geometric growth [14]. Local hemodynamics regulated by the flow conditions drives aneurysm

remodeling through pathobiology determining future geometry and at the same time geometry instantaneously determines flow conditions [14]. Aneurysm growth would result in geometric enlargement until it reaches homeostasis or rupture.

According to Meng H et al, though rupture episode itself could be triggered by temporary pressure and/or frequency surge and wall failure, propensity of aneurysm rupture is resulted by biological wall degradation interceded by the interaction between hemodynamics and pathobiology with time [14]. Frösen J et al has reported that unruptured saccular IA wall is characterized by myointimal hyperplasia and organizing thrombus, while ruptured aneurysm wall is typified by a decellularized, degenerated matrix and a poorly organized luminal thrombus [2]. An insightful explanation of the role of hemodynamics in the 3 phases of IA natural history (initiation, growth and rupture) has been proposed by Meng H et al, where the authors point out that high WSS and positive WSS gradient trigger aneurysm initiation while aberrant hemodynamics of both low and high WSS induce aneurysm growth and rupture via two distinctive biologic pathways: 1) low WSS and high oscillatory shear index triggering inflammatory cell mediated destructive remodeling. 2) high WSS and positive WSS gradient triggering mural cell mediated destructive remodeling [14].

Hemodynamic analysis methods

Hemodynamics is mainly evaluated using computational fluid dynamics (CFD) [15-16] for intracranial arteries and IAs. Another means of hemodynamic analysis is magnetic resonance fluid dynamics (MRFD) [17-19] which is performed utilizing 3D cine phase-contrast MR imaging (3D cine PC MRI), which is concurrently referred to as 4D Flow MRI [20-21]. Although CFD is often used in neuroradiology owing to its higher

spatial resolution, it requires extensive calculation time along with substantial computational power [22] and notably CFD depends on many assumptions regarding fluid properties and its boundary [21]. On the other hand, MRFD is a real measurement which requires lesser time and effort despite its limited spatial resolution in the smaller vessels [21,23]. Even though Doppler ultrasound can also be used to measure blood flow velocity, its user dependency, limited insonation angles and unidirectional velocity encoding have hindered its higher spatiotemporal resolution in comparison to flow sensitive MRI, which enables hemodynamic analysis without limitations of anatomic coverage or flow directions [24]. Specifically, 3D cine PC MRI has surpassed 2D cine PC MRI mainly due to its full spatial and temporal coverage of area of interest, ability to provide higher spatial resolution in all three dimensions without compensating signal to noise ratio and ability to provide velocity multiplanar reformation with three directional vector field plots and velocity profiles mapped onto selected planes of interest [20].

Current dilemma of IAs

The most serious consequence of IAs is their rupture, which is the most common cause of non-traumatic subarachnoid hemorrhage (SAH) [25]. SAH is associated with high rates of mortality besides resultant cognitive and functional disabilities [26-27]. Epidemiological studies carried out in different regions of the world have reported median mortality rates of SAH ranging from 27% to 44% and global cognitive impairment rate associated with SAH ~ 20% [28]. A common observation regarding the detected IAs is that the majority of aneurysms does not rupture and appear to be stable over lifetime. An annual rupture rate of 0.95% has been reported for unruptured cerebral aneurysms in a Japanese cohort which excluded patients who underwent treatment [29] whereas an

average annual rupture incidence of 1.1% has been reported for a Finnish population in which none of the IAs underwent treatment [30]. Clinical risk factors affecting natural course of IAs are claimed to be aneurysm size, shape, location, patient age, smoking status, hypertension, alcohol consumption, family history and polycystic kidney disease [29-33].

Recent advancements in neurovascular imaging, particularly in MR imaging, and the broadened use have increased the detection of incidentally found IAs [34-36] besides the concurrent upgrades in treatment techniques. As a result, many unruptured IAs have become candidates for treatment. However, treatment of unruptured IAs carries the risk of associated morbidity and mortality rates regardless of their benefits. Park HK et al [37] have reported procedure related neurologic morbidity rate of 1.4% and mortality rate of 1.4%, associated with endovascular treatment of unruptured IAs whereas Fennell VS et al [38] have reported 6.4% of morbidity rate and 1.6% of mortality rate for unruptured IAs which underwent endovascular treatment. Another study based on patient registries in Scandinavia has reported a one-year mortality rate of 2.7% for patients with unruptured IAs [39]. Hence deciding which aneurysms should undergo treatment is of vital importance. This decision making in treatment is mainly based on the aneurysm size and location in the clinical setting despite other suggested clinical risk factors and hemodynamic parameters for IA rupture. In this context, published evidence for IA natural course suggest that aneurysms located in anterior or posterior circulations and the ones greater than 7 mm in size are more prone to rupture [29-30]. Nevertheless, the fact that small aneurysms also rupture and that some larger aneurysms appear to be stable over time in follow-up studies irrespective of their location makes this decision making for treatment quite controversial and necessitate systematic and profound analysis to be carried out with respect to rupture risk assessment.

Current status of research in IA rupture risk assessment

Several recent studies have investigated morphological and hemodynamic parameters to assess the rupture risk of IAs and have found significant results with respect to aspect ratio [40], size ratio [41], presence of blebs [29], nonsphericity index [42], inflow concentration index [43], energy loss [44], pressure loss coefficient [45] and wall shear stress derivatives [7-12]. Particularly, following investigators have discovered significant morphological and hemodynamic biomarkers in their respective studies: Xiang J et al [9] have reported that hemodynamics is equally important as morphology in discriminating IA rupture as they had found size ratio, WSS and oscillatory shear index (OSI) as IA rupture discriminants; Takao H et al [45], have suggested pressure loss coefficient as a potential parameter to predict future IA rupture; Jing L et al [7] have found large aspect ratio and low WSS mean to be independently associated with the rupture status of multiple IAs; Skodvin, T. Ø et al [46] have disclosed that hemodynamics at the time of diagnosis are different in aneurysms that later rupture than in those that remain unruptured and have further suggested that increased low shear area might be an early predictor of IA rupture; Amigo N & Valencia A [10] have observed size ratio, systolic WSS, diastolic WSS and relative residence time (RRT) as significant parameters to assess rupture risk of cerebral aneurysms; Chung BJ et al [8] have revealed that unstable and ruptured aneurysms have more complex flows with concentrated WSS and are larger, more elongated and irregular than stable aneurysms, independent of aneurysm location, patient gender and age. However, all of these studies are based on CFD analysis and none of these studies had used patient specific inflow-outflow boundary conditions for the analysis which is a major limitation. In addition, to our knowledge, no rigorous IA rupture risk assessment study has been reported that utilizes MRFD analysis with representative

larger samples rather than case reports.

Purpose of the present study

The aim of our study was to evaluate in-vivo hemodynamic and morphological biomarkers of IAs, using MRFD and MR based patient specific CFD in order to assess the risk of rupture.

Materials and Methods

This study was approved by relevant institutional review boards and informed consent had been taken from the patients whose image data were utilized. 48 IAs (10 ruptured aneurysms and 38 unruptured aneurysms) were retrospectively analyzed in the present study, with the intention of identifying morphological and hemodynamic biomarkers for aneurysm rupture using MRFD and CFD utilizing patient specific vessel geometry and patient specific inflow-outflow boundary conditions.

Study subjects

Our data base consisted of 297 IAs of 203 patients who had been followed up after the initial diagnosis. 3D time-of-flight magnetic resonance angiography (3D TOF MRA) and 3D cine phase-contrast magnetic resonance imaging (3D cine PC MRI) data of IAs which had been followed up at our three affiliated institutes contributing to our database from 2005 to 2018 were reviewed in the current investigation. Each case had undergone 3D TOF MRA and 3D cine PC MRI at least once during the follow-up. Saccular IAs, consisting both lateral wall and bifurcation type were included in the study. Of 297 aneurysms, 7 aneurysms had undergone 3D cine PC MRI before rupture enabling

the analysis of pre-rupture status exclusively while 4 cases had undergone 3D cine PC MRI immediately or few days after rupture. Careful inspection was carried out to confirm vasospasm or any geometric change caused by the rupture for these 4 cases. As a result, 3 cases were included in the study and 1 case was excluded due to the presence of vasospasm. Thus 10 ruptured aneurysms were selected to "ruptured group". Average time duration from image acquisition to rupture date was 56 months for the aneurysms which ruptured during follow-up and average time duration from aneurysm rupture to imaging date was 3 days for the aneurysms without follow-up before rupture.

The aneurysms those did not rupture during the follow-up were screened for inclusion to the "unruptured group". Inclusion criteria for the "unruptured group" were the aneurysms located in similar sites as the ruptured group with no evidence of SAH and with at least 20 months of follow-up time. This resulted in 182 aneurysms. Subsequent exclusion criteria were the aneurysms which underwent endovascular treatment (109), giant IAs (size >10mm) or aneurysms of size less than 3mm (27), aneurysms with arteriosclerotic changes (2), aneurysms with improper velocity encoding (VENC) settings or narrow field of view (FOV) (6). Accordingly, 144 aneurysms had to be excluded from the "unruptured group", resulting in 38 aneurysms which met all the inclusion and exclusion criteria. Average follow up time for these 38 unruptured aneurysms was 86

months. Patient clinical information on gender, ethnicity, history of prior subarachnoid hemorrhage, presence of hypertension, diabetes, polycystic kidney disease, connective tissue disease, family history of IAs or SAH, smoking status and alcohol use were acquired for known risk factors of aneurysm rupture for the 48 cases included in the study.

Imaging methods and parameters

1.5T MR scanner with 8-channel neurovascular array coil and two 3T MR scanners with 8-channel and 12-channel neurovascular array coils were utilized in image acquisition. 3 ruptured and 6 unruptured aneurysms included in the study had been imaged using 1.5T MR scanner whereas 6 ruptured and 22 unruptured aneurysms had been imaged using 3T MR scanner with 8-channel neurovascular array coil. The other 3T MR scanner with 12-channel neurovascular array coil had been utilized in the image acquisition of 1 ruptured and 10 unruptured aneurysms in the study. The imaging parameters of 3D TOF MR angiography and 3D cine PC MR imaging are shown in *Table 1*.

Table 1. MR imaging parameters used in the study

	1.5T MR scanner (Signa Infinity Twin speed with Excite, GE Healthcare) with an 8-channel head array coil (Slew rate, 77 T/m/s)		**3T MR scanner (Signa HDx 3T, GE Healthcare) with an 8-channel neurovascular array coil (Slew rate, 150 T/m/s)**		**3T MR scanner (Verio 3T, Siemens) with a 12-channel head matrix coil (Slew rate, 200 T/m/s)**	
Sequence	3D TOF MRA	3D cine PC MR	3D TOF MRA	3D cine PC MR	3D TOF MRA	3D cine PC MR
Slice orientation	transaxial	transaxial	transaxial	transaxial	transaxial	transaxial
TR (ms)/TE (ms)/NEX	30/2.6/1	9/3/1	26/3.1/1	5.3/2.4/1	25.0/4.67/1	7.81/3.88/1
Flip angle (degrees)	15	15	20	15	18	15
FOV (mm)	200×200×105	160×160×32	192×192×102	160×160×32	160×160×72	160×160×30-40
Matrix	320×224×176 (512×512×176*)	160×160×40 (256×256×40*)	512×192×204 (512×512×204*)	160×160×32 (256×256×64*)	320×320×144 (640×640×144*)	160×160×30-40 (320×320×30-40*)
Voxel size (mm^3)	0.63×0.89×0.6 (0.39×0.39×0.6*)	1×1×0.8 (0.63×0.63×0.8*)	0.38×1×0.5 (0.38×0.38×0.5*)	1×1×1 (0.63×0.63×0.5*)	0.5×0.5×0.5 (0.25×0.25×0.5*)	1×1×1 (0.5×0.5×1*)
VENC (cm/s)	NA	100	NA	120	NA	120
Number of phases	NA	20	NA	20	NA	19**
Parallel imaging	NA	ARC	NA	ARC	NA	GRAPPA
Acceleration factor	NA	2	NA	2	NA	2
View per segment	NA	4	NA	4	NA	1-2
ECG gating or triggering	NA	retrospective	NA	retrospective	NA	prospective
Bandwidth (Hz/pixel)	122	488	122	488	220	473
Acquisition time	4 m 48 s	6 m 58 s	5 m 39 s	9 m 36 s	11 min 51 s	26 min 21 s**

*ARC, Autocalibrating Reconstruction for Cartesian sampling; ECG, electrocardiogram; FOV, field of view; GRAPPA, GeneRAlized auto calibrating Partially Parallel Acquisitions; MRA, magnetic resonance angiography; NA, not applicable; NEX, number of excitation; PC, phase-contrast; T, tesla; TOF, time of flight; TR, repetition time; TE, echo time; VENC, velocity encoding; *, zero-filled interpolation processing; **, average*

Magnetic Resonance Fluid Dynamic (MRFD) Analysis

Blood flow analysis software, Flova, (Renaissance of Technology Corporation, Hamamatsu, Japan) was utilized for MRFD analysis. First patient-specific vascular geometries were obtained from 3D TOF MRA data. Region growing method and marching cube method were utilized to segment vessel wall geometry. Next 3D velocity

vectors obtained from 3D cine PC MRI were loaded over the extracted vessel geometry using Flova *(Figure 1)*.

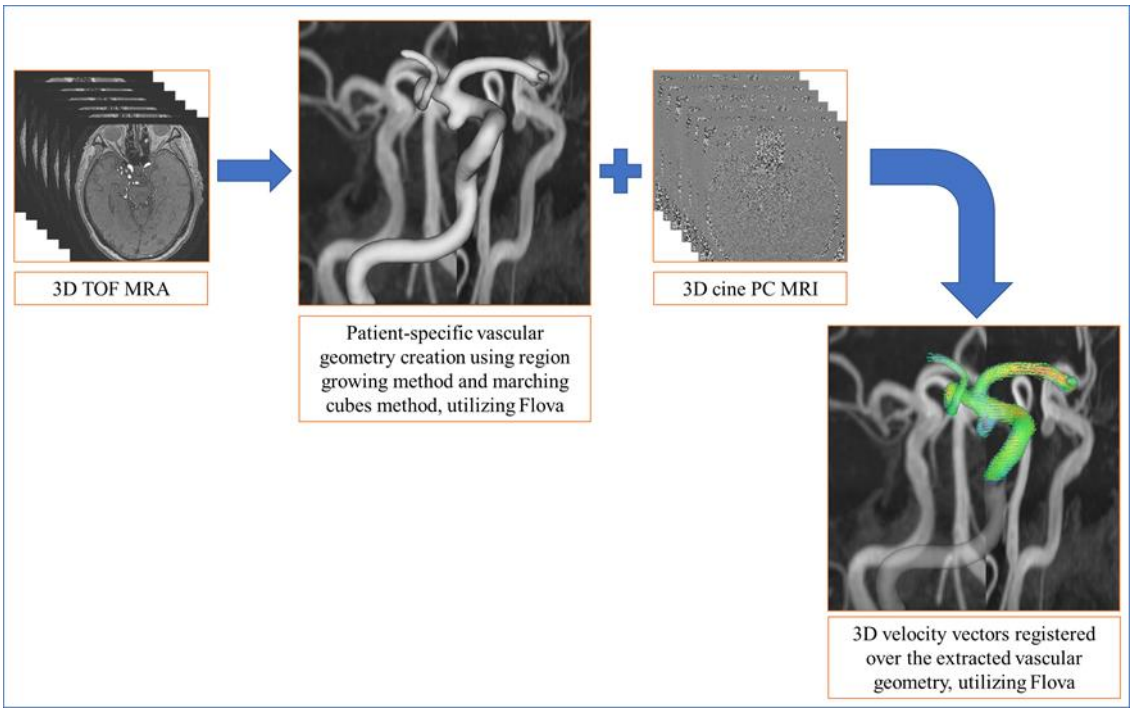

Figure 1. MRFD analysis: obtaining vascular geometry and registration of 3D velocity vectors

Phase correction processing was performed while registering velocity vectors and phase encoding directions were adjusted accordingly. Manual corrections of vessel surface position were made when and if there was spatial misregistration between the vessel surface and flow velocity vectors. Once the optimum registration of 3D flow velocity vectors over the vessel geometry was attained *(Figure 2)* geometric measurements of the aneurysm and its parent artery were carried out. Subsequently,

analysis planes for the biomarker calculation were set enabling the calculation of hemodynamic parameters *(Figure 3)*.

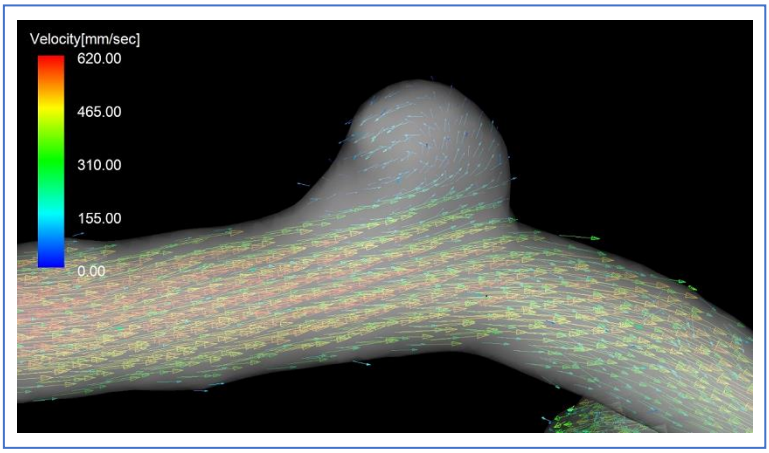

Figure 2. Illustration of vessel geometry and blood flow velocity vector distribution in and around a representative aneurysm

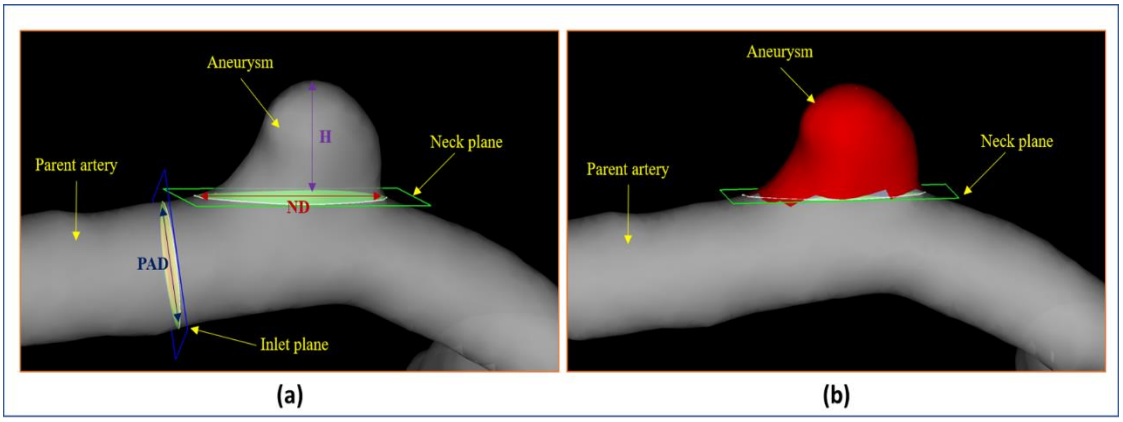

Figure 3. Illustration of geometric measurements and analysis planes setting in and around an aneurysm for biomarker calculation

Figure 3(a): Illustration of aneurysm neck, inlet plane and geometric measurements. H, maximum perpendicular height of the aneurysm; ND, Aneurysm neck diameter; PAD, Parent artery diameter

Figure 3(b): Illustration of aneurysm volume. Aneurysm volume is denoted by the red highlighted voxels, which represents the vessel volume above the neck plane.

Computational fluid dynamic (CFD) analysis

3D vascular geometries, which were reconstructed using 3D TOF MRA data utilizing Flova, were exported in stereolithography (STL) format to create tetrahedral meshes using ICEM CFD version 14.5 (ANSYS, Canonsburg, Pennsylvania, USA). Maximum edge length was defined as 0.3 mm and minimal was 0.1 mm for each mesh. Surface prism mesh consisted of 4 prism mesh layers. The thickness of the outermost layer mesh was 0.04 mm and spreading rate was 1.2. The inlet and outlet regions of vascular geometries were extended in order to maintain laminar flow. Volume flow rates of vessels were obtained from MRFD analysis to be used as patient specific inlet and outlet boundary conditions. CFD solver software CFX version14.5 (ANSYS, Canonsburg, Pennsylvania, USA) was used to compute velocity biomarkers by solving Navier-Stokes equation. Liquid was set as incompressible Newtonian fluid, density was set to 1054 kg/m^3 and dynamic viscosity was set to 3.8 mPa·s. Vascular walls were assumed to be rigid and non-slip. Intervals of cardiac cycles were divided into 100 steps. Two cardiac cycles were simulated and the results of the second cycle were taken for the calculation of hemodynamic biomarkers to ensure numeric stability. Analysis planes placement and hemodynamic biomarker calculation were proceeded using CFD-Post 14.5 (ANSYS, Canonsburg, Pennsylvania, USA).

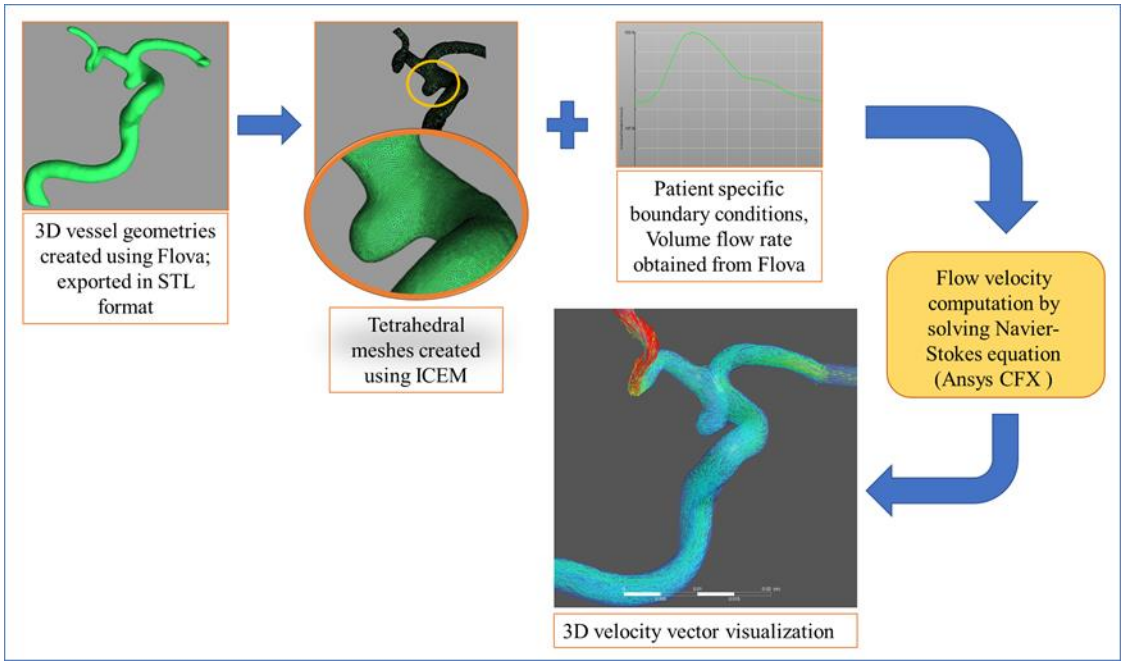

Figure 4. CFD analysis: importing vascular geometry, mesh creation, velocity vector computations and visualization of 3D velocity vectors

Morphological biomarkers

Six morphological biomarkers denoting aneurysm size and shape measures, namely size, volume, aspect ratio, size ratio, presence of blebs and nonsphericity index (NSI) were investigated in this study. Size was defined as the maximum diameter of the aneurysm and both size and aneurysm volume were measured using MRFD analysis. Aspect ratio, a measure of aneurysm ellipticity, which has been initially proposed by Ujiie H, *et al* [40] was defined as the ratio of the maximum perpendicular height to the neck diameter of the aneurysm in the present study. Size ratio, originally proposed by Dhar S, *et al* [41], was defined as the ratio of the maximum aneurysm height to the parent vessel

diameter. Aneurysm blebs were defined as irregular protrusions [29] or lobulations of the aneurysm wall and the presence or absence of blebs were confirmed after careful examination of created 3D vessel geometries, by an experienced neuroradiologist and the main investigator of the study. Nonsphericity index (NSI), which was introduced by Raghavan ML, Ma B, & Harbaugh RE [42], is a collective measure of undulations and ellipticity of the aneurysm and was calculated using the following equation;

$$NSI = 1 - (18\pi)^{1/3} \cdot \frac{V^{2/3}}{S}$$

where V and S are volume and surface area of the aneurysm. NSI was investigated in the present study to represent quantification of aneurysm surface irregularity while taking the shape of aneurysm into account.

Hemodynamic biomarkers

Four main hemodynamic parameters were investigated in this study. One parameter, the inflow concentration index (ICI), was chosen as a velocity biomarker. ICI, which was proposed by Cebral JR et al, represents the degree of concentration of the flow stream entering the aneurysm [43] and was calculated using the following equation;

$$\mathrm{ICI} = \frac{\mathrm{Q_{in}}/\mathrm{A_{in}}}{\mathrm{Q_v}/\mathrm{A_o}}$$

where Q_{in} is flow rate into the aneurysm (m^3/s), Q_v is the flow rate in the parent

artery (m^3/s), A_{in} is the area of inflow region of the aneurysm (m^2) and A_o is the area of the ostium surface (m^2).

The other three parameters were derivatives of wall sheer stress (WSS), which is defined as the multiplication of fluid viscosity and shearing velocity of neighboring vascular wall [6]. Shearing velocity is calculated by dividing velocity along the wall by distance from wall to the velocity measuring point. WSS related parameters evaluated in this study were time averaged wall shear stress (TAWSS) [7-10], oscillatory shear index (OSI) [11] and relative residence time (RRT) [12].

TAWSS (Pa) was calculated as the average of the WSS(τ_ω) during a cardiac cycle T. Further spatially minimum (TAWSS.min), spatially maximum (TAWSS.max) and spatially average TAWSS (TAWSS.ave) were calculated over the aneurysm region.

$$\text{TAWSS} = \frac{1}{T}\int_0^T |\tau_\omega(\vec{x}, t)|\, dt$$

OSI, a dimensionless quantity which measures the directional change of WSS during the cardiac cycle, was calculated using the following formula [11];

$$\text{OSI} = \frac{1}{2}\left(1 - \frac{\int_0^T \tau_\omega(\vec{x}, t)\, dt}{\int_0^T |\tau_\omega(\vec{x}, t)|\, dt}\right)$$

As with TAWSS, spatially minimum (OSI.min), spatially maximum (OSI.max) and spatially averaged (OSI.ave) values of OSI were calculated over the aneurysm region.

RRT is the relative residence time of blood near the wall of the aneurysm [12], which was calculated as the following equation;

$$\mathrm{RRT} = \frac{1}{\{(1 - 2 \times OSI)\mathrm{TAWSS}\}}$$

RRT was further computed to obtain spatially minimum (RRT.min), spatially maximum (RRT.max) and spatially averaged (RRT.ave) values.

Statistical Analysis

IBM SPSS Statistics (version 25) was used for the statistical analysis in order to evaluate the biomarkers between ruptured and unruptured groups. The known risk factors for aneurysm rupture and the presence of blebs between the two groups were compared using Fisher's Exact test. Unpaired Student's t-test and Mann-Whitney U test were conducted as univariate analysis to detect any significant differences in the biomarkers between these two groups. Shapiro-Wilk test was used to test the normality of data; if the null hypothesis in Shapiro-Wilk test was rejected, Mann-Whitney U test was done and these data are reported as medians with inter quartile range (IQR); and, if the null hypothesis in Shapiro-Wilk test was not rejected, unpaired Student's t-test was done and these data are reported as means with standard deviation (SD). Furthermore, receiver operating characteristic (ROC) analysis was performed for the selected statistically

significant biomarkers, and area under the curve (AUC) values and optimal threshold using Yuden index were calculated for them. Logistic regression analysis (using backward stepwise elimination method) was also conducted as multivariate analysis with aneurysm rupture status as the dependent variable for the biomarkers which attained statistical significance in the univariate analysis. Logistic regression was performed separately for the morphological biomarkers, the hemodynamic biomarkers derived from MRFD analysis, and for the hemodynamic biomarkers derived from CFD analysis. Correlations between MRFD and CFD based hemodynamic biomarkers were assessed by Spearman's correlation coefficients. All reported p-values were two-sided, and p-values below 0.05 were considered to indicate statistical significance for all statistical tests.

Results

Forty-eight IAs categorized as ruptured (10 aneurysms) and unruptured (38 aneurysms) were included in the analysis. Ruptured group consisted of 1 anterior communicating artery (AComA) aneurysm, 1 middle cerebral artery (MCA) aneurysm, 3 internal carotid-posterior communicating artery (ICPComA) aneurysms, 1 internal carotid-anterior choroidal artery (ICAnt.ChoA) aneurysm, 1 basilar artery tip (BA Tip) aneurysm, 2 basilar artery-superior cerebellar artery (BASCA) aneurysms and 1 vertebral artery-posterior inferior cerebellar artery (VAPICA) aneurysm (*Table 2*).

Table 2. Size of the aneurysms in the ruptured group

Ruptured aneurysm	Size of the aneurysm (mm)
AComA An.	6.70
MCA An.	4.38
ICPComA An. #1	11.75
ICPComA An. #2	5.34
ICPComA An. #3	3.77
ICAnt.ChoA An.	8.83
BA Tip An.	13.75
BASCA An. #1	5.04
BASCA An. #2	10.89
VAPICA An.	8.62

AComA An., anterior communicating artery aneurysm; MCA An., middle cerebral artery aneurysm; ICPComA An., internal carotid-posterior communicating artery aneurysm; ICAnt.ChoA An., internal carotid-anterior choroidal artery aneurysm; BA Tip An., basilar artery tip aneurysm; BASCA An., basilar artery-superior cerebellar artery aneurysms; VAPICA An., vertebral artery-posterior inferior cerebellar artery aneurysm.

Unruptured group comprised 7 AComA aneurysms, 16 MCA aneurysms, 7 ICPComA aneurysms, 2 ICAnt.ChoA aneurysms, 5 BA Tip aneurysms and 1 BASCA aneurysm.

With respect to the clinically known risk factors for aneurysm rupture, our study did not reveal any statistical significance for any of the assessed risk factors. All the subjects in this study belonged to one ethnicity and none of them have had prior subarachnoid hemorrhage (SAH), connective tissue disease, polycystic kidney disease or family history of aneurysm rupture or SAH. Also, presence of hypertension, diabetes, alcohol intake and tobacco intake were not significant with reference to aneurysm rupture. Although female gender was prominent in the ruptured group, gender did not gain statistical significance as a rupture risk discriminant in the present study (*Table 3*).

Morphological biomarkers

Results of univariate analysis for five morphological biomarkers (size, volume, aspect ratio, size ratio and NSI) are presented in *Table 4*, where the biomarkers for which the null hypothesis in Shapiro-Wilk test was not rejected are listed as mean ± SD and the biomarkers for which the null hypothesis in Shapiro-Wilk test was rejected are as median (IQR). The aneurysm size ($p = 0.021$), volume ($p = 0.035$) and size ratio ($p = 0.039$) were found to be significantly different between the ruptured and unruptured aneurysms,

whereas aspect ratio and NSI were not statistically significantly different.

Table 3. Comparison of clinically known risk factors between the ruptured and unruptured groups

Clinical Characteristics		Unruptured Group (n=38)	Ruptured group (n=10)	p value
Gender	Female	24	9	0.140
	Male	14	1	
Ethnicity	all subjects belong to one ethnicity			NA
Prior SAH	Present	0	0	NA
Hypertension	No	11	4	0.703
	Present	27	6	
Tobacco intake	No	33	7	0.336
	Yes	5	3	
Diabetes	No	35	9	1.000
	Present	3	1	
Alcohol intake	No	32	9	1.000
	Yes	6	1	
Connective tissue disease	Present	0	0	NA
Polycystic kidney disease	Present	0	0	NA
Family history of aneurysm or SAH	Present	0	0	NA

NA, not applicable. SAH, subarachnoid hemorrhage
p value corresponds to the Fisher's-Exact Test statistic and statistical significance is set at $p < 0.05$.

With respect to the presence of blebs, 15 aneurysms with blebs were found in the unruptured group and 5 aneurysms presented blebs in the ruptured group. Thus, Fishers exact test could not reveal a statistical significance (p= 0.721) for the presence of blebs in discriminating aneurysm rupture (*Table 5*).

Table 4. Morphological biomarkers - univariate analysis

Biomarker	Unruptured Group	Ruptured Group	p value
An. size	4.975 (2.09)	7.66 (6.23)	0.021*
An. volume	28.038 (42.01)	175.118 (288.66)	0.035*
Aspect ratio	0.601 (0.29)	0.849 (0.58)	0.121
Size ratio	1.048 ± 0.43	1.408 ± 0.62	0.039*
NSI	0.353 ± 0.06	0.329 ± 0.083	0.282

Parametric variables are denoted with mean ± SD and nonparametric variables with median (IQR). An. size, size of the aneurysm; An. volume, volume of the aneurysm; NSI, nonsphericity index. Unit of An. Size is mm. Unit of An. Volume is mm^3.
**statistically significant at $p<0.05$*

Table 5. Morphological biomarkers – categorical variable analysis

Biomarker		Unruptured Group (n=38)	Ruptured group (n=10)	p value
Presence of blebs	Present	15	5	0.721
	Absent	23	5	

p value corresponds to the Fisher's-Exact Test statistic and statistical significance is set at $p < 0.05$.

ROC analysis (*Figure 5*) revealed AUC values greater than 0.7 for the three significant morphological biomarkers which are presented in *Table 7* along with the identified optimal threshold, sensitivity and specificity values.

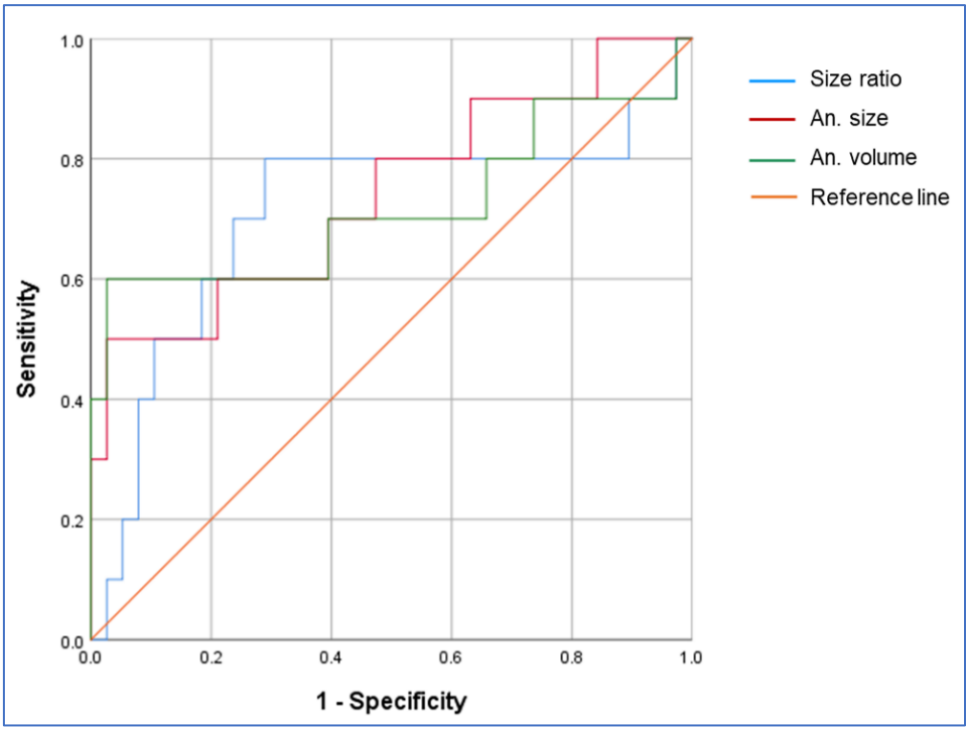

Figure 5. ROC curves representing significant morphological biomarkers to distinguish aneurysm rupture

ROC curves, receiver operating characteristic analysis curves; An. size, size of the aneurysm; An. volume, volume of the aneurysm

Hemodynamic biomarkers

The univariate analysis results for the hemodynamic biomarkers are presented in *Table 6*, where the variables are reported in the same way as in *Table 4*. The MRFD analysis results of hemodynamic biomarkers indicated that the ruptured aneurysms had significantly higher OSI (OSI.max, p = 0.037) and significantly higher RRT (RRT.ave, p = 0.035) compared with the unruptured aneurysms. Correspondingly, the CFD analysis results demonstrated statistically significant differences between the two groups with respect to OSI (OSI.ave, p = 0.008; OSI.max, p = 0.01) and RRT (RRT.max, p = 0.045).

However, the other hemodynamic biomarkers (ICI and TAWSS) were not statistically significantly different either in MRFD or in CFD analysis.

Table 6. Hemodynamic biomarkers using MRFD and CFD -Univariate analysis

Biomarker	MRFD analysis			CFD analysis		
	Unruptured Group	Ruptured Group	p value	Unruptured Group	Ruptured Group	p value
ICI	0.436 (0.67)	0.791 (1.04)	0.310	0.842 (0.92)	1.140 (0.80)	0.477
TAWSS.ave	1.353 ± 0.39	1.157 ± 0.41	0.173	2.442 (2.72)	1.852 (2.05)	0.275
TAWSS.max	3.003 ± 1.04	2.868 ± 1.01	0.714	12.412 ± 5.98	13.687 ± 9.15	0.596
TAWSS.min	0.416 ± 0.15	0.331 ± .134	0.103	0.096 (0.24)	0.049 (0.12)	0.104
OSI.ave	0.075 (0.08)	0.120 (0.08)	0.141	0.011 (0.01)	0.026 (0.02)	0.008*
OSI.max	0.442 (0.08)	0.475 (0.05)	0.037*	0.288 (0.15)	0.405 (0.08)	0.010*
OSI.min	0.0019 (0.01)	0.0016 (0.003)	0.264	0.0001 (0.000)	0.0001 (0.000)	0.879
RRT.ave	1.111 (0.58)	2.012 (1.26)	0.035*	0.879 (1.52)	1.533 (4.54)	0.187
RRT.max	12.377 (19.70)	28.453 (73.24)	0.054	20.277 (62.58)	100.477 (133.72)	0.045*
RRT.min	0.382 (0.20)	0.390 (0.21)	0.630	0.079 (0.07)	0.089 (0.08)	0.526

Parametric variables are denoted with mean ± SD and nonparametric variables with median (IQR). MRFD, magnetic resonance fluid dynamics; CFD, computational fluid dynamics; ICI, inflow concentration index; TAWSS, time averaged wall shear stress; TAWSS.ave, spatially averaged TAWSS; TAWSS.max, spatially maximum TAWSS; TAWSS.min, spatially minimum TAWSS; OSI, oscillatory shear index; OSI.ave, spatially averaged OSI; OSI.max, spatially maximum OSI; OSI.min, spatially minimum OSI; RRT, relative residence time; RRT.ave, spatially averaged RRT; RRT.max, spatially maximum RRT; RRT.min, spatially minimum RRT. Unit of TAWSS is Pa.

**statistically significant at $p<0.05$*

Figure 6 and *Figure 7* graphically illustrate the distribution of OSI over the 10 ruptured aneurysms and selected unruptured aneurysms with similar location and shape to match the ruptured aneurysms using MRFD and CFD analyses.

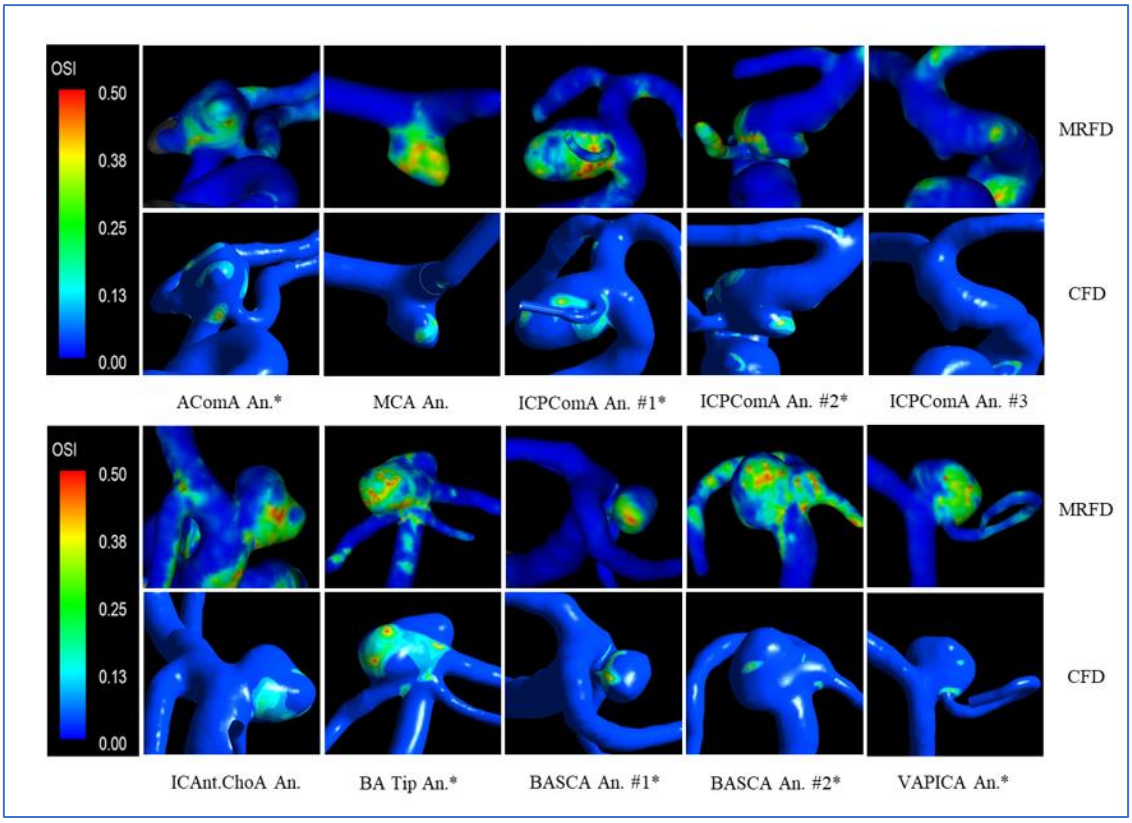

Figure 6. Distribution of OSI for the 10 ruptured aneurysms using MRFD and CFD analyses
Larger areas of elevated OSI are noticeable in these ruptured aneurysms compared to the representative unruptured aneurysms demonstrated in Figure 7.
MRFD, magnetic resonance fluid dynamics; CFD, computational fluid dynamics; OSI, oscillatory shear index; AComA An., anterior communicating artery aneurysm; ICPComA An., internal carotid-posterior communicating artery aneurysm; ICAnt.ChoA An., internal carotid-anterior choroidal artery aneurysm; MCA An., middle cerebral artery aneurysm; BA Tip An., basilar artery tip aneurysm; BASCA An., basilar artery-superior cerebellar artery aneurysms; VAPICA An., vertebral artery-posterior inferior cerebellar artery aneurysm
** denotes the aneurysms which underwent 3D cine PC MRI before rupture enabling the assessment of pre-rupture hemodynamics.*

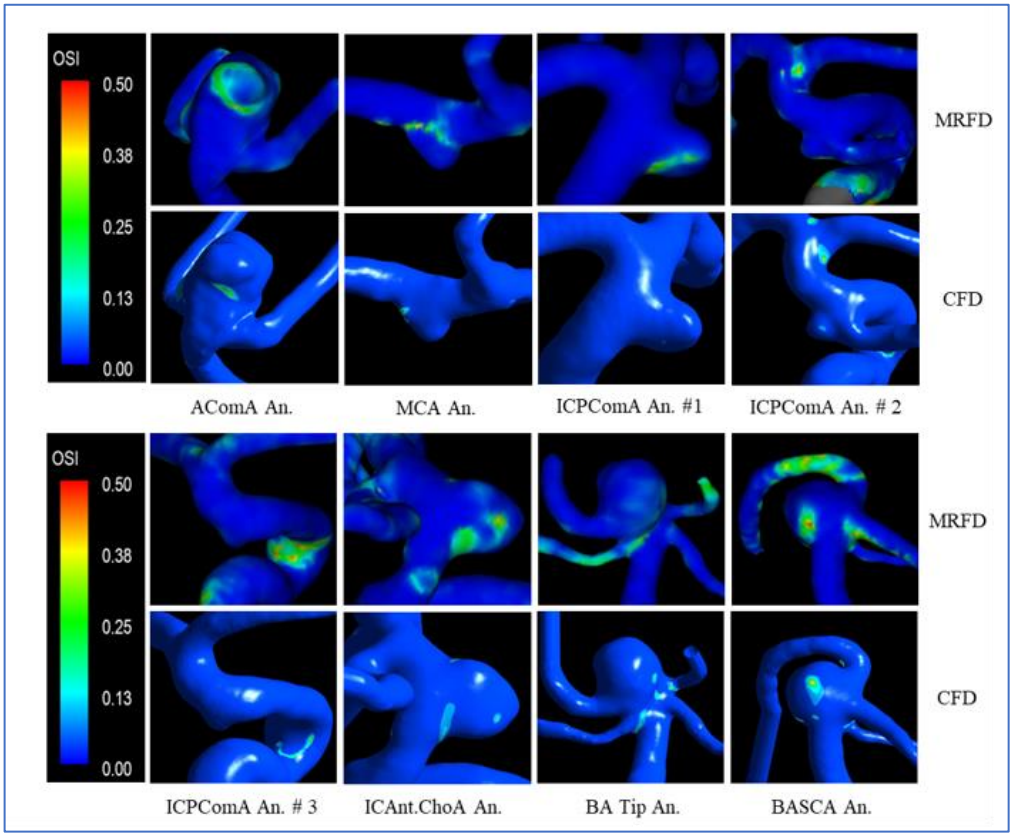

Figure 7. Distribution of OSI for representative unruptured aneurysms with similar location and geometry as the ruptured aneurysms using MRFD and CFD analyses

Unruptured group included only one BASCA An. and did not include any VAPICA An. due to non-availability.

MRFD, magnetic resonance fluid dynamics; CFD, computational fluid dynamics; AComA An., anterior communicating artery aneurysm; ICPComA An., internal carotid-posterior communicating artery aneurysm; ICAnt.ChoA An., internal carotid-anterior choroidal artery aneurysm; MCA An., middle cerebral artery aneurysm; BA Tip An., basilar artery tip aneurysm; BASCA An., basilar artery-superior cerebellar artery aneurysms; VAPICA An., vertebral artery-posterior inferior cerebellar artery aneurysm

For the hemodynamic biomarkers which indicated statistically significant differences between the two groups, ROC analysis (*Figure 8*) revealed AUC curve values greater than 0.7 and *Table 7* provides identified threshold values with respective sensitivity and specificity values.

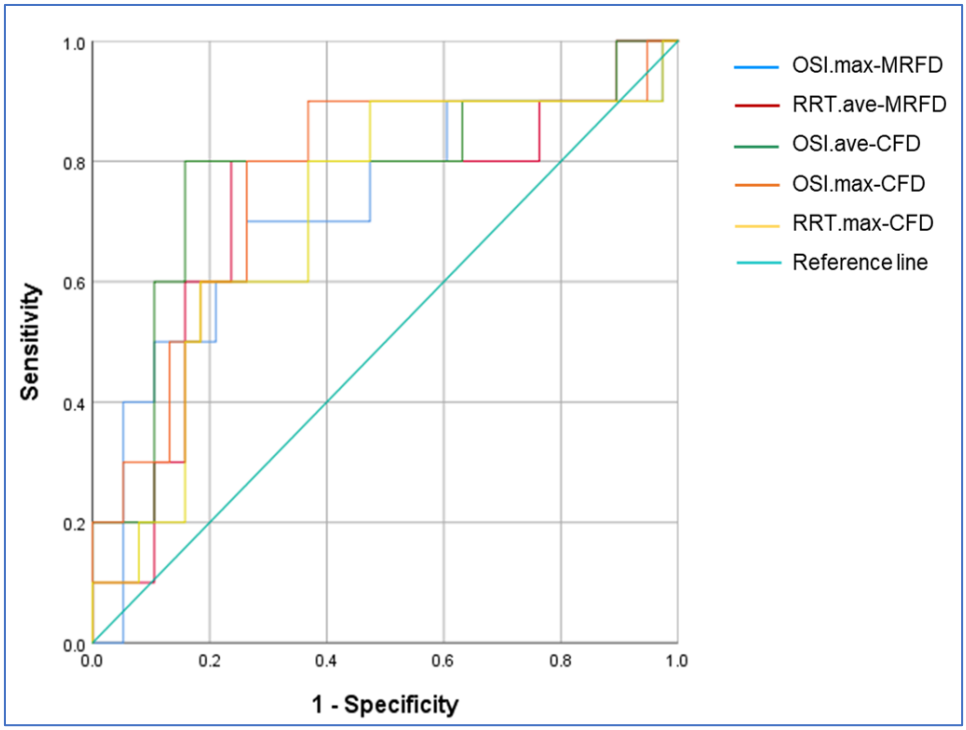

Figure 8. ROC curves representing significant hemodynamic biomarkers to distinguish aneurysm rupture

ROC curves, receiver operating characteristic analysis curves; MRFD, magnetic resonance fluid dynamics; CFD, computational fluid dynamics; OSI, oscillatory shear index; RRT, relative residence time; OSI.max-MRFD, spatially maximum OSI obtained using MRFD; RRT.ave-MRFD, spatially averaged RRT obtained using MRFD; OSI.ave-CFD, spatially averaged OSI obtained using CFD; OSI.max-CFD, spatially maximum OSI obtained using CFD; RRT.max-CFD, spatially maximum RRT obtained using CFD

Table 7. AUC and optimal thresholds for the significant biomarkers

Biomarker	AUC	Threshold (Sensitivity, Specificity)
An. size	0.739	8.525 (0.50, 0.97)
An. volume	0.718	152.315 (0.60, 0.97)
Size ratio	0.708	1.188 (0.80, 0.71)
OSI.max-MRFD	0.716	0.459 (0.70, 0.74)
RRT.ave-MRFD	0.718	1.494 (0.80, 0.76)
OSI.ave-CFD	0.774	0.021 (0.80, 0.84)
OSI.max-CFD	0.766	0.358 (0.80, 0.74)
RRT.max-CFD	0.708	31.719 (0.80, 0.63)

AUC, area under the curve of receiver operating characteristic analysis curve; An. size, size of the aneurysm; An. volume, volume of the aneurysm; OSI, oscillatory shear index; RRT, relative residence time; OSI.max-MRFD, spatially maximum OSI obtained using MRFD; RRT.ave-MRFD, spatially averaged RRT obtained using MRFD; OSI.ave-CFD, spatially averaged OSI obtained using CFD; OSI.max-CFD, spatially maximum OSI obtained using CFD; RRT.max-CFD, spatially maximum RRT obtained using CFD. Threshold values were obtained using Yuden Index.

Multivariate analysis

Binary logistic regression analysis was performed to identify independent predictive biomarkers for aneurysm rupture using backward stepwise method. Significant morphological biomarkers and hemodynamic biomarkers were separately regressed in order to determine predictive models. With respect to the morphological biomarkers, the volume of aneurysm (*An.Vol*) [OR, 1.015; 95% CI, 1.004-1.026] was the only significant

predictor of aneurysm rupture which was retained in the model (AUC, 0.718; 95% CI, 0.491–0.946) and its odds of aneurysm rupture (Odd_M) was estimated to be;

$$Odd_M = e^{0.015(An.Vol)-2.652}$$

In the hemodynamic biomarkers derived from the CFD analysis, average OSI (*OSI.ave*) [OR, $1.942e^{+32}$; 95% CI, 8706.389-$4.333e^{+60}$] was the only significant predictor of aneurysm rupture which was retained in the logistic regression model (AUC, 0.774; 95% CI, 0.586–0.961) and its odds of aneurysm rupture (Odd_H) was estimated to be;

$$Odd_H = e^{74.347(OSI.ave)-2.775}$$

However, there were no any significant predictors of aneurysm rupture among the MRFD based hemodynamic biomarkers with respect to multivariate regression analysis.

Correlations between MRFD and CFD based hemodynamic biomarkers

Spearman's rank correlation coefficients revealed strong positive monotonic correlations between MRFD and CFD for ICI, and moderate positive monotonic correlations for TAWSS.ave, TAWSS.min, OSI.ave, OSI.max, RRT.ave, and RRT.max (*Table 8*). The other biomarkers were unable to reveal such significant correlations. However, all the biomarkers which were found to be significant risk factors for aneurysm rupture showed moderate correlations between MRFD and CFD.

Table 8. Correlation coefficients between MRFD and CFD based hemodynamic biomarkers

Biomarker	Correlation coefficient	p value
ICI	0.863*	0.000
TAWSS.ave	0.413*	0.004
TAWSS.max	0.257	0.078
TAWSS.min	0.506*	0.000
OSI.ave	0.318*	0.028
OSI.max	0.419*	0.003
OSI.min	-0.030	0.842
RRT.ave	0.447*	0.001
RRT.max	0.434*	0.002
RRT.min	0.171	0.245

MRFD, magnetic resonance fluid dynamics; CFD, computational fluid dynamics; ICI, inflow concentration index;TAWSS, time averaged wall shear stress; TAWSS.ave, spatially averaged TAWSS; TAWSS.max, spatially maximum TAWSS; TAWSS.min, spatially minimum TAWSS; OSI, oscillatory shear index; OSI.ave, spatially averaged OSI; OSI.max, spatially maximum OSI; OSI.min, spatially minimum OSI; RRT, relative residence time; RRT.ave, spatially averaged RRT; RRT.max, spatially maximum RRT; RRT.min, spatially minimum RRT. Correlations were assessed using Spearman's correlation coefficients.

** Correlation is significant at p<0.05.*

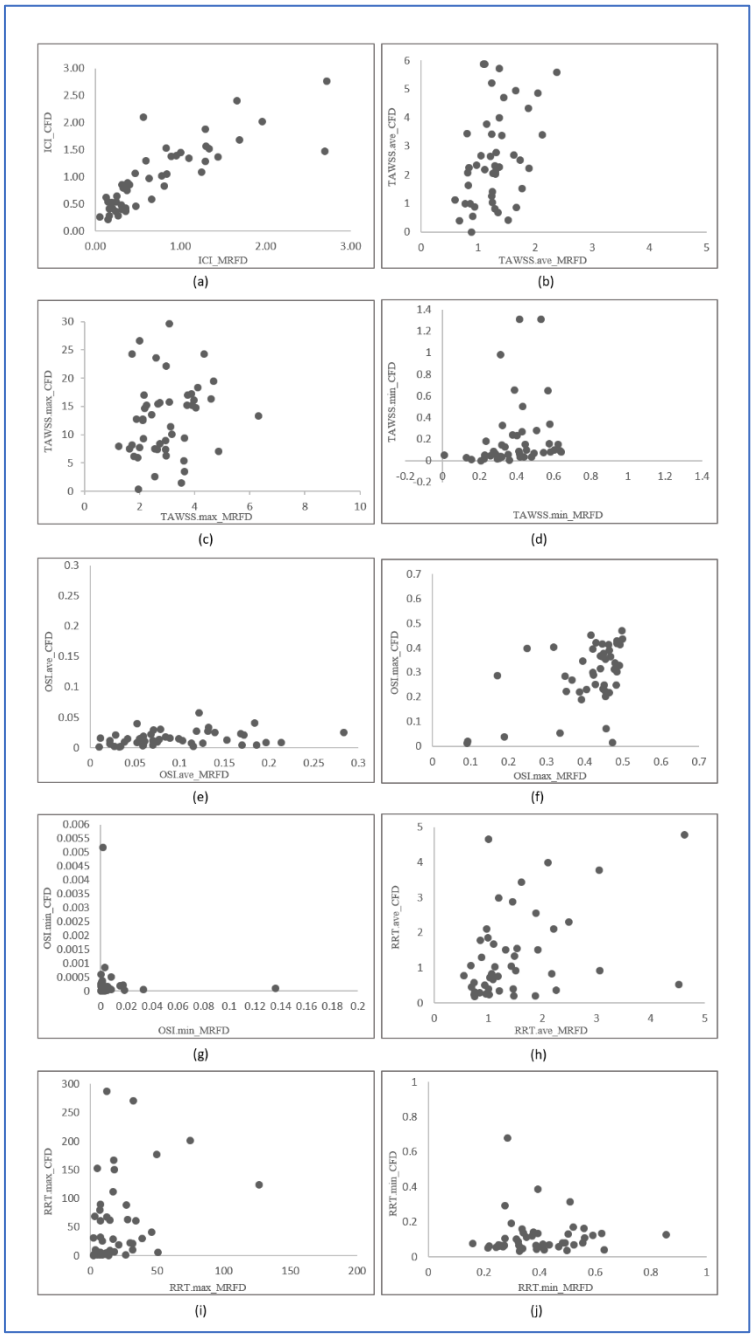

Figure 9. Scatterplots of hemodynamic biomarkers obtained from MRFD and CFD

Figure 9. (a)-(j), represents scatterplots denoting the correlations obtained for ICI, TAWSS.ave, TAWSS.max, TAWSS.min, OSI.ave, OSI.max, OSI.min, RRT.ave, RRT.max and RRT.min between MRFD and CFD respectively.

MRFD, magnetic resonance fluid dynamics; CFD, computational fluid dynamics; ICI, inflow concentration index; TAWSS, time averaged wall shear stress; TAWSS.ave, spatially averaged TAWSS; TAWSS.max, spatially maximum TAWSS; TAWSS.min, spatially minimum TAWSS; OSI, oscillatory shear index; OSI.ave, spatially averaged OSI; OSI.max, spatially maximum OSI; OSI.min, spatially minimum OSI; RRT, relative residence time; RRT.ave, spatially averaged RRT; RRT.max, spatially maximum RRT; RRT.min, spatially minimum RRT.

Discussion

Intracranial aneurysm rupture risk assessment using morphological and hemodynamic biomarkers has been the focus of many recent studies. Despite the fact that treatment decisions are mainly based on aneurysm size and location in the clinical setting, increased attention has been given to hemodynamics in and around aneurysms in research. Our study investigated both morphological and hemodynamic biomarkers with the aim of identifying possible rupture risk discriminants. Although there are many studies which had assessed IA rupture risk assessment using CFD, no published evidence is found for a comprehensive study that utilized MRFD in this context, to the best of our knowledge. Also, no published evidence can be found for IA rupture risk assessment study which had utilized patient specific inflow-outflow boundary conditions for CFD analysis together with MRFD analysis besides few studies which had compared inflow hemodynamics of IAs using patient specific CFD and MRFD [22, 47]. Hence, we analyzed hemodynamic biomarkers using MRFD analysis in addition to CFD analysis which utilized patient specific vessel geometry as well as patient specific inflow-outflow boundary conditions derived from 3D cine PC MRI. Our study results revealed that the ruptured aneurysms had significantly larger aneurysm size, volume, and size ratio, oscillatory shear index

(OSI) and relative residence time (RRT) compared with the unruptured aneurysms. Specifically, in terms of hemodynamic analysis, MRFD showed statistically significant differences in OSI and RRT comparable with CFD analysis.

Regarding the clinically known risk factors for aneurysm rupture, our study did not show any statistical significance comparable to the study results of the UCAS Japan study [29]. The average size of a ruptured aneurysm in our study was 7.91mm and the most common location for rupture was internal carotid-posterior communicating artery. UCAS Japan investigators had reported that aneurysms larger than 7 mm and the ones located in the posterior and anterior communicating arteries were more prone to rupture. Despite the fact that our study sample is too small because our ruptured group consisted of only 10 ruptured aneurysms and the unruptured group 38 aneurysms, we could observe similar pattern in epidemiological characteristics in comparison to the UCAS Japan study. However, these epidemiological characteristics could have been affected by the fact that presumably higher risk aneurysms have already undergone treatment resulting an inadequate representation in the rupture risk assessment.

With reference to the morphological biomarkers investigated in the present study, aneurysm size, volume and size ratio showed statistically significant differences between the ruptured and unruptured aneurysms in the univariate analysis, while only aneurysm

volume became a significant predictor of aneurysm rupture in multivariate analysis. These results imply that larger aneurysm size and volume can have a significant effect on aneurysm rupture. However, our ruptured group consisted of 2 aneurysms of size less than 5 mm and 5 aneurysms of size less than 7mm (*Table 2*). Furthermore, despite our ruptured group included 3 aneurysms of size greater than 10mm, giant aneurysms were excluded from the unruptured group to avoid segmentation and hemodynamic analysis restrictions due to the parent artery obstruction caused by the aneurysm. This might have induced some sort of under representation for the medium or small size aneurysms in the ruptured group. Nevertheless, similar findings with respect to size and size ratio of aneurysms as rupture discriminants have been reported by Jing L *et al* [7], Chung B.J *et al* [8], Xiang J *et al* [9] and Amigo N & Valencia. A [10]. The aneurysm volume, which had the most significant effect on rupture risk assessment in our study, have not been studied as an independent morphological biomarker in most of the studies. The aspect ratio, presence of blebs and nonsphericity index (NSI) did not gain statistical significance in our study comparable to Amigo N & Valencia. A [10] but in contrast to several other studies [7-9], [40-42].

In relation to the investigated hemodynamic biomarkers, OSI and RRT were significantly different between the ruptured group and the unruptured group of aneurysms

suggesting higher blood oscillations and longer resident times near aneurysm wall can distinguish aneurysm rupture. The longer the time blood spends inside the aneurysm, the slower and circulatory its flow. Hence these two biomarkers are interrelated. According to the multivariate analysis, OSI was the only significant biomarker for predicting aneurysm rupture risk. It can be speculated that higher blood oscillations for longer time inside the aneurysm is triggering aneurysm wall degeneration and thereby instigate rupture. Meng H *et al* has proposed that this aneurysm wall degeneration due to high OSI could have been triggered by an inflammatory-cell-mediated destructive remodeling [14]. Similar results have been found by Xiang J *et al* and Amigo N & Valencia A, with respect to OSI and RRT [9-10] as rupture discriminants. Despite the fact that both OSI and RRT are derivatives of WSS, our study was unable to reveal any statistical significance with reference to WSS. However, several studies have reported WSS in the aneurysm as a significant parameter in the rupture risk assessment [7-10]. In addition, ICI was unable to show a significant effect on the aneurysm rupture risk in the present study in contrast to the initial findings reported by Cebral J.R *et al* [43]. With respect to another two hemodynamic biomarkers, although we attempted the analysis of EL [44] and PLc [45], confounding results were observed possibly due to the distinctive ways of approximation of static pressure variable by the fluid dynamic analysis software. Those results are not

presented in this study as further scrutiny is warranted regarding the biomarker definitions and way of analysis.

With respect to the observed correlations in hemodynamic biomarkers between MRFD and CFD analyses, TAWSS.ave, TAWSS.min, OSI.ave, OSI.max, RRT.ave, and RRT.max exhibited moderate positive monotonic correlations whereas ICI verified strong correlation (*Table 8*). However, the rest of the 3 hemodynamic biomarkers could not reveal such correlations. van Ooij et al has reported that WSS magnitude estimated by PC MRI is lower compared to CFD and the effect to be more pronounced in systole [19]. This could have affected the correlation results of WSS related biomarkers in our study as well. It should be noted that ICI, which mainly depends on flow velocity, had revealed strong correlation between MRFD and CFD. The spatial minimum values of both OSI and RRT could not reveal any correlation possibly due to the fact that CFD simulations are able to output very small numbers compared to MRFD software. Furthermore, it can be reflected that increased spatial resolution in MRFD along with larger sample size would result better correlations between MRFD and CFD.

In the view of hemodynamic analysis methods, although CFD is recognized as the standard criterion, it depends on many assumptions and substantial time is needed for the simulations to be run in addition to the considerable time and effort needed in the pre

and post analysis methods in obtaining biomarkers. On the other hand, MRFD needs lesser time and personnel effort despite its low resolution compared to CFD in assessing arteries with small caliber [23]. It is reflected that MRFD is more feasible in the clinical setting whereas CFD would be appropriate for the experimental and research setting. In the present study, the statistically significant hemodynamic biomarkers between the ruptured and unruptured groups showed the same pattern in both MRFD and CFD based results. Hence in the context of assessing IA rupture risk, MRFD could be utilized.

In comparison to the available published data on IA rupture risk assessments, an important merit of the present study is utilizing both MRFD and CFD analyses for the hemodynamic biomarker assessment. Moreover, the use of patient specific inflow-outflow boundary conditions validates our CFD results in contrast to using representative normal subject's velocity profile along with additional assumptions for all the cases. Also, despite the fact that current study is not a case control study like the ones reported by Skodvin, T. Ø *et al* [46] and Chung B.J *et al* [8] our unruptured group was scrutinized to match the locations with the ruptured group. Yet the unruptured group was unable to represent VAPICA aneurysm, due to non-availability of an unruptured aneurysm in the same location in our data base.

Even though 3D rotational angiography (3DRA) and computed tomography

angiography (CTA) have been generally used for vessel geometry in morphological and hemodynamic analyses of IAs due to its high spatial resolution, we utilized 3D TOF MRA for vessel geometry creation. For one reason, the noninvasiveness and comparatively low cost of 3D TOF MRA has made it the most widely used imaging method for IAs during follow-up and on the other hand published evidence not only suggest that CT, MRI and 3DRA adequately reproduce aneurysm geometry and allow meaningful CFD analysis but also revealed that MRI is 2.5 times better than CT with respect to mean reconstruction errors [48]. In addition, Ren Y, et al [49] has reported that CTA and MRA have no significant differences in reproducing IA geometry. We did not use magnitude images derived from 3D cine PC MRI as the vessel geometry and rather opted for 3D TOF MRA for two reasons. First, the spatial resolution and signal intensity of vessels of 3D TOF MRA were superior than those of magnitude images derived from 3D cine PC MRI. Second, we employed thicker slab 3D TOF MRA data, as CFD analysis necessitates geometric information of upper and lower stream vessels. However, the use of 3D TOF MRA instead of magnitude image of 3D cine PC MRI resulted in occasional misregistration of velocity vectors, which had to be manually corrected.

Although seven out of the ten ruptured aneurysms had undergone 3D cine PC MRI before rupture, the rest of the three aneurysms were imaged immediately or few days

after rupture. In spite of our careful scrutiny to exclude any geometric change or vasospasm for these three cases, this could be a limitation of our study. Another limitation of our study could be not discriminating stable and unstable aneurysms in the unruptured group. However, according to a recent study carried out by Chung B.J *et al* [8], which compared the hemodynamics and geometries of stable, unstable, and ruptured aneurysms, collectively analyzing stable and unstable aneurysms together as unruptured aneurysms against ruptured aneurysms permit the characterization of biomarkers due to higher prevalence of stable aneurysms in an unruptured population. One more limitation of our study could be incorporating MR imaging obtained at both 1.5T and 3T field strengths for the hemodynamic analysis. The fact that quality of 3D cine PC MRI performed at 3T field strength is higher than 3D cine PC MRI at 1.5T [50] might have affected the quantitative comparison of hemodynamic biomarkers to some extent.

Conclusion

Both morphological and hemodynamic biomarkers have significant influence on intracranial aneurysm rupture. Aneurysm size, volume, size ratio, oscillatory shear index and relative residence time could be potential biomarkers to assess aneurysm rupture risk where aneurysm volume and oscillatory shear index are the most significant predictors of aneurysm rupture.

References

1. Vlak MH, Algra A, Brandenburg R, Rinkel GJ. Prevalence of unruptured intracranial aneurysms, with emphasis on sex, age, comorbidity, country, and time period: a systematic review and meta-analysis. Lancet Neurol 2011; 10:626-636.

2. Frösen J, Tulamo R, Paetau A, et. al. Saccular intracranial aneurysm: pathology and mechanisms. Acta Neuropathol. 2012; 123:773-786.

3. Hacein-Bey L, Provenzale JM. Current imaging assessment and treatment of intracranial aneurysms. AJR Am J Roentgenol. 2011; 196:32-44.

4. Park SH, Yim MB, Lee CY, Kim E, Son EI. Intracranial Fusiform Aneurysms: It's Pathogenesis, Clinical Characteristics and Managements. J Korean Neurosurg Soc. 2008;44:116–123.

5. Secomb TW. Hemodynamics. Compr Physiol. 2016; 6:975-1003.

6. Malek AM, Alper SL, Izumo S. Hemodynamic shear stress and its role in atherosclerosis. JAMA 1999; 282:2035-2042.

7. Jing L, Fan J, Wang Y, et al. Morphologic and Hemodynamic Analysis in the Patients with Multiple Intracranial Aneurysms: Ruptured versus Unruptured. PLoS One 2015; 10:e0132494.

8. Chung BJ, Mut F, Putman CM, et al. Identification of Hostile Hemodynamics and Geometries of Cerebral Aneurysms: A Case-Control Study. AJNR Am J Neuroradiol. 2018; 39:1860-1866.

9. Xiang J, Natarajan SK, Tremmel M, et al. Hemodynamic-morphologic discriminants for intracranial aneurysm rupture. Stroke 2011; 42:144-152.

10. Amigo N & Valencia ÁJ. Determining Significant Morphological and Hemodynamic Parameters to Assess the Rupture Risk of Cerebral Aneurysms. J. Med. Biol. Eng 2019; 39:329-335.

11. He X, Ku DN. Pulsatile flow in the human left coronary artery bifurcation: average conditions. J Biomech Eng 1996; 118:74-82.

12. Himburg HA, Grzybowski DM, Hazel AL, LaMack JA, Li XM, Friedman MH. Spatial comparison between wall shear stress measures and porcine arterial endothelial permeability. Am J Physiol Heart Circ Physiol 2004; 286:H1916- H1922.

13. Brisman JL, Song JK, Newell DW. Cerebral aneurysms. N Engl J Med. 2006 Aug 31;355(9):928-39. Review. PubMed PMID: 16943405.

14. Meng H, Tutino VM, Xiang J, Siddiqui A. High WSS or low WSS? Complex interactions of hemodynamics with intracranial aneurysm initiation, growth, and rupture: toward a unifying hypothesis. AJNR Am J Neuroradiol 2014; 35:1254-1262.

15. Steinman DA. Image-based computational fluid dynamics modeling in realistic arterial geometries. Ann Biomed Eng 2002; 30:483-497.

16. Cebral JR, Yim PJ, Löhner R, Soto O, Choyke PL. Blood flow modeling in carotid arteries with computational fluid dynamics and MR imaging. Acad Radiol 2002; 9:1286-1299.

17. Isoda H, Ohkura Y, Kosugi T, et al. In vivo hemodynamic analysis of intracranial aneurysms obtained by magnetic resonance fluid dynamics (MRFD) based on time-resolved three-dimensional phase-contrast MRI. Neuroradiology 2010; 52:921-928.

18. Futami K, Nambu I, Kitabayashi T, et al. Inflow hemodynamics evaluated by using four-dimensional flow magnetic resonance imaging and the size ratio of unruptured cerebral aneurysms. Neuroradiology 2017; 59:411-418.

19. van Ooij P, Potters WV, Guédon A, et al. Wall shear stress estimated with phase contrast MRI in an in vitro and in vivo intracranial aneurysm. J Magn Reson Imaging 2013; 38:876-84.

20. Markl M, Chan FP, Alley MT, et al. Time-resolved three-dimensional phase-contrast MRI. J Magn Reson Imaging 2003; 7:499-506.

21. Markl M, Frydrychowicz A, Kozerke S, Hope M, Wieben O. 4D flow MRI. J Magn Reson Imaging. 2012; 36:1015-1036.

22. van Ooij P, Schneiders JJ, Marquering HA, et al. 3D cine phase-contrast MRI at 3T in intracranial aneurysms compared with patient-specific computational fluid dynamics. AJNR Am J Neuroradiol. 2013; 34:1785-1791.

23. Fukuyama A, Isoda H, Morita K, et al. Influence of Spatial Resolution in Three-dimensional Cine Phase Contrast Magnetic Resonance Imaging on the Accuracy of Hemodynamic Analysis. Magn Reson Med Sci 2017; 16:311-316.

24. Stalder AF, Russe MF, Frydrychowicz A, et al. Quantitative 2D and 3D phase contrast MRI: optimized analysis of blood flow and vessel wall parameters. Magn Reson Med. 2008; 60:1218-1231.

25. van Gijn J, Rinkel GJ. Subarachnoid haemorrhage: diagnosis, causes and management. Brain 2001; 124:249-278.

26. Lantigua H, Ortega-Gutierrez S, Schmidt JM, et al. Subarachnoid hemorrhage: who dies, and why? Crit Care 2015; 19:309.

27. Al-Khindi T, Macdonald RL, Schweizer TA. Cognitive and functional outcome after aneurysmal subarachnoid hemorrhage. Stroke 2010; 41:e519- e536.

28. Connolly ES Jr, Rabinstein AA, Carhuapoma JR, et al. Guidelines for the management of aneurysmal subarachnoid hemorrhage: a guideline for healthcare

professionals from the American Heart Association/American Stroke Association. Stroke. 2012; 43:1711-1737.

29. UCAS Japan Investigators, Morita A, Kirino T, Hashi K, et al. The natural course of unruptured cerebral aneurysms in a Japanese cohort. N Engl J Med 2012; 366:2474-2482.

30. Juvela S, Poussa K, Lehto H, Porras M. Natural history of unruptured intracranial aneurysms: a long-term follow-up study. Stroke 2013; 44:2414-2421.

31. Sonobe M, Yamazaki T, Yonekura M, Kikuchi H. Small unruptured intracranial aneurysm verification study: SUAVe study, Japan. Stroke 2010; 41:1969-77.

32. Can A, Castro VM, Ozdemir YH, et al. Alcohol Consumption and Aneurysmal Subarachnoid Hemorrhage. Transl Stroke Res 2018; 9:13-19.

33. Nurmonen HJ, Huttunen T, Huttunen J, et al. Polycystic kidney disease among 4,436 intracranial aneurysm patients from a defined population. Neurology 2017; 89:1852-1859.

34. Deutschmann HA, Augustin M, Simbrunner J, Unger B, et al. Diagnostic accuracy of 3D time-of-flight MR angiography compared with digital subtraction angiography for follow-up of coiled intracranial aneurysms: influence of aneurysm size. AJNR Am J Neuroradiol. 2007; 28:628-634.

35. Tang PH, Hui F, Sitoh YY. Intracranial aneurysm detection with 3T magnetic resonance angiography. Ann Acad Med Singapore. 2007; 36:388-393.

36. Okahara M, Kiyosue H, Yamashita M, et al. Diagnostic accuracy of magnetic resonance angiography for cerebral aneurysms in correlation with 3D-digital subtraction angiographic images: a study of 133 aneurysms. Stroke. 2002; 33:1803-1808.

37. Park HK, Horowitz M, Jungreis C, et al. Periprocedural morbidity and mortality associated with endovascular treatment of intracranial aneurysms. AJNR Am J Neuroradiol. 2005; 26:506-514.

38. Fennell VS, Martirosyan NL, Palejwala SK, Lemole GM Jr, Dumont TM. Morbidity and mortality of patients with endovascularly treated intracerebral aneurysms: does physician specialty matter? J Neurosurg. 2016; 124:13-17.

39. Lindekleiv H, Mathiesen EB, Førde OH, Wilsgaard T, Ingebrigtsen T. Hospital volume and 1-year mortality after treatment of intracranial aneurysms: a study based on patient registries in Scandinavia. J Neurosurg. 2015; 123:631-637.

40. Ujiie H, Tamano Y, Sasaki K, Hori T. Is the aspect ratio a reliable index for predicting the rupture of a saccular aneurysm? Neurosurgery 2001; 48:495-503.

41. Dhar S, Tremmel M, Mocco J, et al. Morphology parameters for intracranial aneurysm rupture risk assessment. Neurosurgery 2008; 63:185-197.

42. Raghavan ML, Ma B, Harbaugh RE. Quantified aneurysm shape and rupture risk. J Neurosurg. 2005; 102:355-62.

43. Cebral JR, Mut F, Weir J, Putman C. Quantitative characterization of the hemodynamic environment in ruptured and unruptured brain aneurysms. AJNR Am J Neuroradiol 2011; 32:145-151.

44. Qian Y, Takao H, Umezu M, Murayama Y. Risk analysis of unruptured aneurysms using computational fluid dynamics technology: preliminary results. AJNR Am J Neuroradiol 2011; 32:1948-1955.

45. Takao H, Murayama Y, Otsuka S, et al. Hemodynamic differences between unruptured and ruptured intracranial aneurysms during observation. Stroke 2012;

43:1436-1439.

46. Skodvin TØ, Evju Ø, Helland CA, Isaksen JG. Rupture prediction of intracranial aneurysms: a nationwide matched case-control study of hemodynamics at the time of diagnosis. J Neurosurg 2018; 129:854-860.

47. Isoda H, Ohkura Y, Kosugi T, et al. Comparison of hemodynamics of intracranial aneurysms between MR fluid dynamics using 3D cine phase-contrast MRI and MR-based computational fluid dynamics. Neuroradiology 2010; 52:913-920.

48. Goubergrits L, Schaller J, Kertzscher U, et al . Reproducibility of image-based analysis of cerebral aneurysm geometry and hemodynamics: an in-vitro study of magnetic resonance imaging, computed tomography, and three-dimensional rotational angiography. J Neurol Surg A Cent Eur Neurosurg 2013; 74:294-302.

49. Ren Y, Chen GZ, Liu Z, et al . Reproducibility of image-based computational models of intracranial aneurysm: a comparison between 3D rotational angiography, CT angiography and MR angiography. Biomed Eng Online 2016; 15:50.

50. Bammer R, Hope TA, Aksoy M, Alley MT. Time-resolved 3D quantitative flow MRI of the major intracranial vessels: initial experience and comparative evaluation at 1.5T and 3.0T in combination with parallel imaging. Magn Reson Med 2007; 57:127-140.

Acknowledgments

First and foremost, I would like to express my sincere gratitude to my advisor, Prof. Haruo Isoda of Brain & Mind Research Center, Nagoya University / Department of Radiological and Medical Laboratory Sciences, Nagoya University Graduate School of Medicine, for his tremendous and continuous guidance and support throughout my Doctor course study. I extend my sincere appreciation for the motivation, encouragement and great patience I received from Prof. Haruo Isoda during my research and in writing this thesis. I could not have imagined of a better advisor and mentor for my Ph.D study.

I would also like to convey my sincere gratitude to Prof. Mitsuru Ikeda of Nagoya University Graduate School of Medicine for his guidance in the statistical analysis of my study. Also, I am thankful for Prof. Yuki Onishi, of Tokyo Institute of Technology, for his advice in the CFD analysis.

My sincere thanks also goes to Mr. Kenta Ishiguro, Mr. Takashi Mizuno and Mr. Shunsuke Tajima who were former students of 'Isoda Laboratory', for their guidance in hemodynamic analysis.

I would like acknowledge Prof. Yasuo Takehara, Prof. Takashi Izumi, Prof. Toshihiko Wakabayashi and Prof. Shinji Naganawa of Nagoya University Graduate School of Medicine and Dr. Masaki Terada, Dr. Chiharu Tanoi and Dr. Takehiro Naito of Iwata City Hospital and Prof. Harumi Sakahara, Dr. Hisaya Hiramatsu, Prof. Hiroki Namba and Dr. Takasuke Ushio of Hamamatsu University School of Medicine for their valuable contributions in the MR image acquisition process.

I would like to thank Mr. Takafumi Kosugi of Renaissance of Technology Corporation for his support in the MRFD analysis and I would like to express my humble appreciation to Dr. Marcus Alley of Stanford University School of Medicine, USA, Mr. Yoshiaki Komori of Siemens Healthcare and Mr. Tetsuya Wakayama of GE Healthcare for their contribution in the technical support of 4D Flow.

Also, my sincere gratitude goes to Japanese Government (MEXT scholarship) for financially facilitating my postgraduate studies in Nagoya University, Japan.

I earnestly thank University of Peradeniya and University Grants Commission of Sri Lanka for granting me study leave in order to pursue my PhD.

My heartfelt thanks goes to my fellow lab-mates for their support I received throughout my study period in research as well as in day-to-day life matters I faced as an international student in Japan.

Last but not the least, my special thanks to my family: specially to my husband for his utmost support and for all the sacrifices he had to bear on behalf of my studies and to my parents and parents-in-law for their immense support throughout my studies.

List of Abbreviations

3D:	three-dimensional
AComA:	anterior communicating artery
ARC:	Autocalibrating Reconstruction for Cartesian sampling
AUC:	area under the curve
BASCA:	basilar artery-superior cerebellar artery
BA Tip:	basilar artery tip
CFD:	computational fluid dynamics
CTA:	computed tomography angiography
ECG:	electrocardiogram
FOV:	field of view
GRAPPA:	GeneRAlized auto calibrating Partially Parallel Acquisitions
IA:	intracranial aneurysm
ICAnt.ChoA:	internal carotid-anterior choroidal artery
ICI:	inflow concentration index
ICPComA:	internal carotid-posterior communicating artery
IQR:	inter quartile range
MCA:	middle cerebral artery
MRA:	magnetic resonance angiography
MRFD:	magnetic resonance fluid dynamics
MRI:	magnetic resonance imaging
NA:	not applicable

ND:	aneurysm neck diameter
NEX:	number of excitations
NSI:	nonsphericity index
OSI:	oscillatory shear index
PAD:	parent artery diameter
PC:	phase-contrast
RA:	rotational angiography
ROC:	receiver operating characteristic
RRT:	relative residence time
SAH:	subarachnoid hemorrhage
SD:	standard deviation
STL:	stereolithography
TAWSS:	time averaged wall shear stress
TE:	echo time
TOF:	time-of-flight
TR:	repetition time
VAPICA:	vertebral artery-posterior inferior cerebellar artery
VENC:	velocity encoding
WSS:	wall shear stress

Research Presentations at International and Local Conferences

1. Perera R, Isoda H, Tajima S, Mizuno S, Terada M, Naito T, Tanoi C, Izumi T, Takehara Y, Wakabayashi T, Sakahara H, Naganawa S. Evaluation of hemodynamic and morphological biomarkers to assess rupture risk of intracranial aneurysms using magnetic resonance fluid dynamics and computational fluid dynamics. In: **The 47th Annual Meeting of the Japanese Society for Magnetic Resonance in Medicine (JSMRM 2019)**, Kumamoto, Japan. September 20 - 22 2019 (Oral presentation)

2. Perera R, Isoda H, Terada M, Tanoi C, Izumi T, Sakahara H. Evaluation of hemodynamic and morphological biomarkers to assess rupture risk of intracranial aneurysms using magnetic resonance fluid dynamics and computational fluid dynamics. In: **The 75th Annual Scientific Congress of Japanese Society of Radiological Technology (JSRT)**, Yokohama, Japan. April 11 -14, 2019 (Oral presentation)

3. Perera R, Isoda H, Mizuno T, Terada M, Naito T, Tanoi C, Izumi T, Sakahara H, Naganawa S. Evaluation of hemodynamic and morphological biomarkers to assess rupture risk of intracranial aneurysms using magnetic resonance fluid dynamics and computational fluid dynamics. In: **25th European Congress of Radiology (ECR),** Vienna, Austria. February27 - March 3, 2019 (Oral presentation)

4. Perera R, Isoda H, Tajima S, Terada M, Naito T, Tanoi C, Izumi T, Takehara Y, Sakahara H, Naganawa S. Evaluation of hemodynamic and morphological biomarkers to assess rupture risk of intracranial aneurysms using magnetic resonance fluid dynamics and computational fluid dynamics. In: **48th annual scientific meeting of the Japanese Society of Neuroradiology**, Kurume, Japan. February 14 - 16, 2019 (Oral presentation)

5. Perera R, Isoda H, Tajima S, Mizuno T, Terada M, Naito T, Tanoi C, Izumi T, Takehara Y, Wakabayashi T, Sakahara H, Naganawa S. Evaluation of hemodynamic and morphological biomarkers to assess rupture risk of intracranial aneurysms using magnetic resonance fluid dynamics and computational fluid dynamics. In: 85th annual scientific meeting of 東海総合画像医学研究会, Nagoya, Japan. January 5, 2019 (Oral presentation)

6. Perera R, Isoda H, Mizuno T, Terada M, Tanoi C, Izumi T, Takehara Y, Wakabayashi T, Sakahara H, Naganawa S. Evaluation of hemodynamic and morphological biomarkers to assess rupture risk of intracranial aneurysms using magnetic resonance fluid dynamics and computational fluid dynamics. In: 3rd annual scientific meeting of **ISMRM- Japanese Chapter**, Nagoya, Japan. December 22 - 23, 2018 (Poster presentation: won the best poster presentation award).

****